Behaviour of asymmetric building with double variable frequency pendulum isolator

D.P. Soni†

Civil Engineering Department, Sardar Vallabhbhai Patel Institute of Technology, Vasad – 388 306, India

B.B. Mistry‡

Engineering College, Tuwa - 389 001, India

V.R. Panchal‡†

Civil Engineering Department, Sardar Vallabhbhai Patel Institute of Technology, Vasad – 388 306, India

(Received May 12, 2009, Accepted October 7, 2009)

Abstract. Presented in this paper is the behaviour of asymmetric building isolated by the double variable frequency pendulum isolator (DVFPI). The DVFPI is an adoption of single variable frequency pendulum isolator (VFPI). The geometry and coefficient of friction of top and bottom sliding surfaces can be unequal. The governing equations of motion of the building-isolation system are derived and solved in incremental form. The analysis duly considers the interaction of frictional forces in the two principal directions developed at each sliding surface of the DVFPI. In order to investigate the behaviour of the base isolation using the DVFPI, the coupled lateral-torsional response is obtained under different parametric variations for a set of six far-fault earthquake ground motions and criterion to optimize its performance is proposed. Further, influences of the initial time period, coefficient of friction and frequency variation factors at the two sliding surfaces are investigated. The numerical results of the extensive parametric study help in understanding the torsional behaviour of the structure isolated with the double sliding surfaces as in the DVFPI. It is found that the performance of the DVFPI can be optimized by designing the top sliding surface initially softer and smoother relative to the bottom one.

Keywords: double variable frequency pendulum isolator; seismic isolation; asymmetric building; eccentricity; torsional coupling.

1. Introduction

Great advances have been made in the development of base isolation technology to protect structures form the hazardous effect of strong earthquakes in the past three decades. A practical

† Research Scholar, E-mail: soni_svit@yahoo.com
‡ Professor, E-mail: bbm_7@yahoo.co.in
‡† Assistant Professor, Corresponding author, E-mail: vijay_svit@yahoo.co.in

base-isolation system typically consists of three basic elements (Buckle 1986): (1) A flexible mounting so that the fundamental period of the total system is lengthened sufficiently to reduce the acceleration response; (2) a supplemental damper or energy-dissipation device so that the relative displacement across the isolation interface can be controlled to a desirable level; and (3) a means of providing rigidity under low load levels such as wind and minor earthquakes. Excellent reviews of the base-isolation concepts and applications are available in published literature (Kelly 1986, Buckle and Mayes 1990, Naeim and Kelly 1999).

Several investigations on the response of base isolated buildings are reported in literature. Most of the analytical works deal with 2-D idealization, which is strictly valid for symmetric buildings. In practice, symmetrical buildings are unlikely to occur and most buildings are unsymmetrical to some extent. The principal candidates leading to asymmetry are unsymmetrical building plan and elevation and unsymmetrical distribution of vertical members and masses on the floors. Compared to the buildings with symmetric configuration, such buildings are more susceptible to lateral loads especially earthquake hazards due to torsional coupling. It is the most important factor that differentiates between 3-D and 2-D idealization of the building and can result in significant response amplifications. Excessive edge deformation due to torsional coupling may cause pounding between closely spaced adjacent buildings. Torsional coupling has been identified as one of the major causes of poor performance or failure of buildings during recent earthquakes. The recognition of this fact has led several researchers to focus their study on the earthquake behaviour of such systems (Lee 1980, Pan and Kelly 1983, Eisenberger and Rutenberg 1986, Zayas *et al*. 1987, Nagarajalah *et al*. 1993a, Nagarajalah *et al*. 1993b, Jangid and Datta 1994, Jangid 1995, Jangid and Kelly 2001, Tena-Colunga and Gomez-Soberon 2002, Pranesh and Sinha 2004, Tena-Colunga and Escamilla-Cruz 2007).

Recently there has been growing interest in the development of double sliding bearing principally owing to two reasons (Fenz and Constantinou 2006): (1) the displacement capacity of such isolator is twice that of the traditional isolator with a single sliding surface of identical plan dimensions permitting it to accommodate large sliding displacement imposed by severe earthquake ground motions, and (2) there is the capability to use sliding surfaces with varying isolator geometry and coefficients of friction at top and bottom sliding surfaces, giving the designer greater flexibility to optimize performance. Taking advantage of these extra design parameters, it may be possible to attain certain benefits in terms of performance that are not currently achievable. Looking to these merits, the double friction pendulum system (DFPS) (Fenz and Constantinou 2006, Tsai *et al*. 2005, Kim and Yun 2005) and the triple friction pendulum system (Fenz and Constantinou 2008a, 2008b) have been designed, tested and have already found numerous applications. These are the mainstream isolation system with thousands of bearing in service. Recently, the authors have proposed the double variable frequency pendulum isolator (DVFPI) (Soni *et al*. 2009). The double and triple friction pendulum bearings are made of well-known friction pendulum system (FPS) (Zayas *et al*. 1987) with spherical sliding surface whereas the DVFPI consist of two variable frequency pendulum isolators (VFPI) (Pranesh and Sinha 2000) having elliptical sliding geometry. Because of the elliptical sliding surface, isolator stiffness of the DVFPI decreases with increase in sliding displacement and therefore, the low-frequency resonant behaviour of the isolator can be attenuated. The similar displacement dependent isolator behaviour can also be achieved by using triple friction pendulum having multiple spherical surfaces rather than using variable curvature sliding surfaces. The triple friction pendulum bearing exhibits adaptive stiffness and damping characteristics. Its behaviour is dictated by the different

combinations of surfaces upon which sliding can occur over the course of motion. As the surfaces upon which sliding occurs change, the stiffness and effective friction change accordingly. The performance of the DVFPI has been examined rigorously when subjected to unilateral, bilateral and triaxial ground excitations (Soni *et al*. 2009, Panchal *et al*. 2009). The torsional behaviour of asymmetric building isolated by the double bearings has not been investigated yet. In view of these, numerical studies have been carried out to examine the torsional behaviour of the DVFPI isolated asymmetric building under bilateral far-fault ground motions by performing 429 computer simulations.

The objectives of this investigation are (a) to present mathematical formulation for the response of a three-dimensional torsionally coupled building isolated with the DVFPI duly considering interaction of frictional forces at both sliding surfaces, (b) to examine the criteria to optimize the performance of the DVFPI, (c) to study the response of asymmetric building for a set of important parametric variations applied individually and in combination, and (d) to examine the influence of isolator parameters on coupled lateral-torsional response.

2. Description of the DVFPI

As mentioned earlier the DVFPI is an adaptation of the VFPI having elliptical sliding surface. Owing to the elliptical sliding surface, oscillation frequency of the VFPI decreases sharply with increase in sliding displacement. Consequently, the dominant frequency of excitation and the isolator frequency are not likely to tune. This property of frequency separation combined with force-softening mechanism of the VFPI makes the isolator performance independent of both amplitude and frequency of excitations (Pranesh and Sinha 2000). The characteristics of the VFPI can be made more effective by introducing a second sliding surface as shown in Fig. 1(a). This device is called the double variable frequency pendulum DFPS isolator. Since sliding is possible on both surfaces, the displacement capacity of the DVFPI is twice that of the traditional VFPI with a single sliding surface of identical plan dimensions. This key feature of the DVFPI permits it to accommodate large sliding displacement produced by severe earthquake ground motions. However, the details and operation of the DVFPI are almost same as the DFPS. The difference between the DFPS and the DVFPI is that the shape of both sliding surfaces in the DFPS is spherical (i.e., constant frequency) whereas that of the DVFPI is non-spherical. The isolator geometry defining upper surface and lower surface of the DVFPI may be unequal. The coefficient of friction of the upper and lower sliding surfaces are also not necessarily equal.

To represent the geometry of the DVFPI, the equation of an ellipse proposed by Pranesh and Sinha (2000) is employed. Accordingly, the geometry of the top and bottom surfaces, respectively can be expressed as

$$z_1 = b_1\left[1 - \frac{\sqrt{d_1^2 + 2d_1 x_1 \mathrm{sgn}(x_1)}}{d_1 + x_1 \mathrm{sgn}(x_1)}\right] \tag{1a}$$

$$z_2 = b_2\left[1 - \frac{\sqrt{d_2^2 + 2d_2 x_2 \mathrm{sgn}(x_2)}}{d_2 + x_2 \mathrm{sgn}(x_2)}\right] \tag{1b}$$

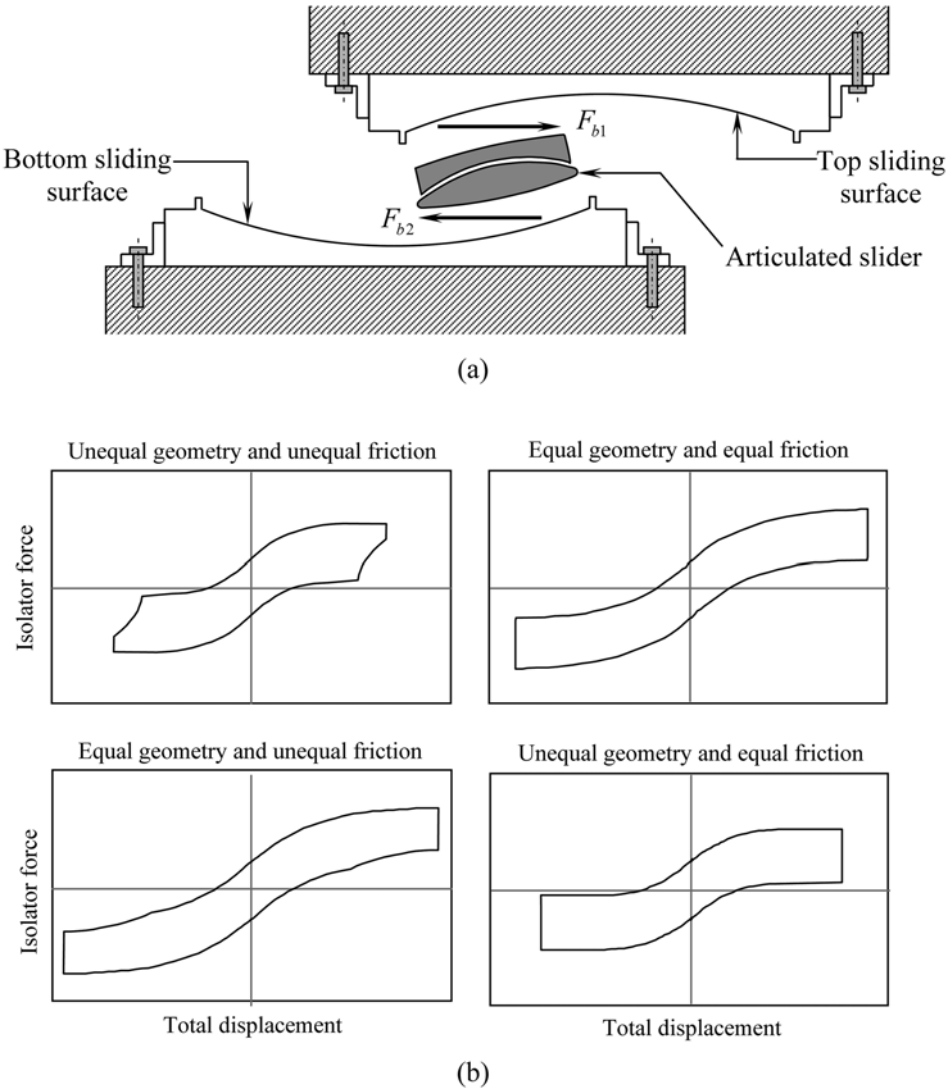

Fig. 1 (a) Schematic details of the DVFPI, and (b) Hysteresis loops for different isolator properties

where b_1 and b_2 are semi-minor axis of the top and bottom sliding surfaces, respectively; d_1 and d_2 are initial value of the semi-major axis of the top and bottom sliding surfaces, respectively; x_1 and x_2 depict the horizontal displacements of the articulated slider relative to the centre of the top and bottom sliding surfaces, respectively; and $\mathrm{sgn}(x_1)$ and $\mathrm{sgn}(x_2)$ are incorporated to maintain the symmetry of the top and bottom sliding surfaces about the central vertical axis. The signum functions have a value of +1 for positive value of sliding displacement and −1 for negative value of sliding displacement.

The isolator forces F_{b1} and F_{b2} being imposed at the top and bottom sliding surfaces can be written as (Pranesh and Sinha 2000)

$$F_{b1} = k_{b1}(x_1)x_1 + F_1 \tag{2a}$$

$$F_{b2} = k_{b2}(x_2)x_2 + F_2 \tag{2b}$$

where,

$$k_{b1}(x_1) = (m_d + m_b)\left(\frac{\omega_{I1}^2}{(1+\bar{r}_1)^2\sqrt{(1+2\bar{r}_1)}}\right) \tag{3a}$$

$$k_{b2}(x_2) = (m_d + m_b + m_s)\left(\frac{\omega_{I2}^2}{(1+\bar{r}_2)^2\sqrt{(1+2\bar{r}_2)}}\right) \tag{3b}$$

$$\omega_{I1} = \sqrt{\frac{gb_1}{d_1^2}}; \qquad \omega_{I2} = \sqrt{\frac{gb_2}{d_2^2}} \tag{4a, 4b}$$

$$\bar{r}_1 = \frac{x_1 \mathrm{sgn}(x_1)}{d_1}; \qquad \bar{r}_2 = \frac{x_2 \mathrm{sgn}(x_2)}{d_2} \tag{5a, 5b}$$

$$F_1 = \mu_1(m_d + m_b)g\,\mathrm{sgn}(\dot{x}_1), \quad F_2 = \mu_2(m_d + m_b + m_s)g\,\mathrm{sgn}(\dot{x}_2) \tag{6a, 6b}$$

here $\bar{r}_1$ and $\bar{r}_2$ are the non-dimensional parameters for the top and bottom sliding surfaces; μ_1 and μ_2 are the coefficients of friction of top and bottom sliding surfaces; m_d, m_b and m_s are the masses of the deck slab, base slab and slider, respectively; F_1 and F_2 are the frictional forces at the top and bottom sliding surfaces, respectively; $k_{b1}(x_1)$ and $k_{b2}(x_2)$ are the displacement dependent stiffnesses (i.e., variable stiffnesses) of top and bottom bearings, respectively; ω_{I1} and ω_{I2} are the initial frequencies of top and bottom bearings, respectively; and g is the acceleration due to gravity.

The total relative displacement of the base mass, u_b (between the centres of the top and bottom sliding surfaces) is the sum of the displacements on the top and bottom surfaces.

$$u_b = x_1 + x_2 \tag{7}$$

Substituting for x_1 and x_2 from Eqs. (2) into Eq. (7), the force-displacement relationship for the DVFPI can be obtained as

$$F_b = \left(\frac{k_{b1}(x_1)k_{b2}(x_2)}{k_{b1}(x_1) + k_{b2}(x_2)}\right)u_b + \left(\frac{F_1 k_{b2}(x_2) + F_2 k_{b1}(x_1)}{k_{b1}(x_1) + k_{b2}(x_2)}\right) = k_c u_b + F_c \tag{8}$$

where k_c and F_c are combined stiffness and combined frictional force of the DVFPI, respectively. Eq. (8) suggests that by defining two separate single VFPI and connecting them in series with a small mass of slider, the overall behaviour of the DVFPI can be obtained. The characteristic force-displacement relationships of the DVFPI are plotted in Fig. 1(b) for different isolator geometry and coefficient of friction of top and bottom sliding surfaces. It is interesting to note that the shape of the hysteretic loops shown in Fig. 1(b) is basically the same as those to be obtained in a ball-in-cone isolation system, which consists of a steel ball sandwiched between two conical steel load plates, as studied and tested by Kasalanati *et al.* (1997). The initial combined time period T_c and combined coefficient of friction μ_c of the DVFPI can be expressed from Eq. (8) as

$$T_c = \sqrt{T_1^2 + T_2^2} \tag{9}$$

$$\mu_c = \frac{\mu_1 T_1^2 + \mu_2 T_2^2}{T_1^2 + T_2^2} \tag{10}$$

where T_1 and T_2 are the initial time period of top and bottom sliding surfaces.

The force-displacement relationship of the DVFPI under bidirectional input motion can be extended from Eqs. (2) as

$$\begin{Bmatrix} F_{bx1} \\ F_{by1} \\ F_{bx2} \\ F_{by2} \end{Bmatrix} = \begin{bmatrix} k_{b1}(r_1) & 0 & 0 & 0 \\ 0 & k_{b1}(r_1) & 0 & 0 \\ 0 & 0 & k_{b2}(r_2) & 0 \\ 0 & 0 & 0 & k_{b2}(r_2) \end{bmatrix} \begin{Bmatrix} x_1 \\ y_1 \\ x_2 \\ y_2 \end{Bmatrix} + \begin{Bmatrix} F_{x1} \\ F_{y1} \\ F_{2x} \\ F_{y2} \end{Bmatrix} \tag{11}$$

where F_{bxj} and F_{byj} are the isolator forces of top and bottom bearing in x- and y-directions, respectively; F_{xj} and F_{yj} are the frictional forces of top and bottom bearing in x- and y-directions, respectively; $r_j = \sqrt{x_j^2 + y_j^2}$ is the relative radial displacement of the slider on jth sliding surface; $k_{bj}(r_j)$ is the displacement dependent isolator stiffness of jth sliding surface as defined in Eqs. (3); and x_j and y_j are the relative displacements of the slider on jth sliding surface in x- and y-directions, respectively.

Due to the elliptical sliding geometry of the DVFPI, the use of an articulated slider as shown in Fig. 1(a) would result in point contact or large concentration of pressure. Under such conditions, the capacity to carry load is limited, sliding friction has unpredictable behavior, frictional heating effects are significant and excessive wear to the sliding surfaces may occur. An alternative configuration to avoid some of these problems is the use of rolling contact, as done in Kasalanati *et al* (1997). This paper presumes that the configuration of Fig. 1(a) is practical and that stable and predictable friction is possible.

3. Structural model

Fig. 2(a) shows a plan of idealized three-dimensional single-story building resting on the DVFPI installed between the base mass and foundation of the building. The assumptions made for the building-isolation system under consideration are as follows:

1. The superstructure is assumed linearly elastic.
2. The friction coefficient of the DVFPI is assumed to be constant and independent of the relative velocity at the sliding interface (Fan *et al*. 1990).
3. Although, a torsional moment develops at each isolator, the contribution of this torsional moment to the total torque exerted at the base mass is insignificant and hence is not included.
4. No overturning or tilting takes place in the superstructure during sliding over the DVFPI.
5. The DVFPI is isotropic (i.e., there is the same isolation period and the coefficient of friction in each of the two principal directions of the motion in the horizontal plane).

The superstructure of the system consists of a rigid deck slab and columns. The lateral dimension of deck slab is d in x-direction and b in y-direction. The rigid deck slab is supported at the edges by

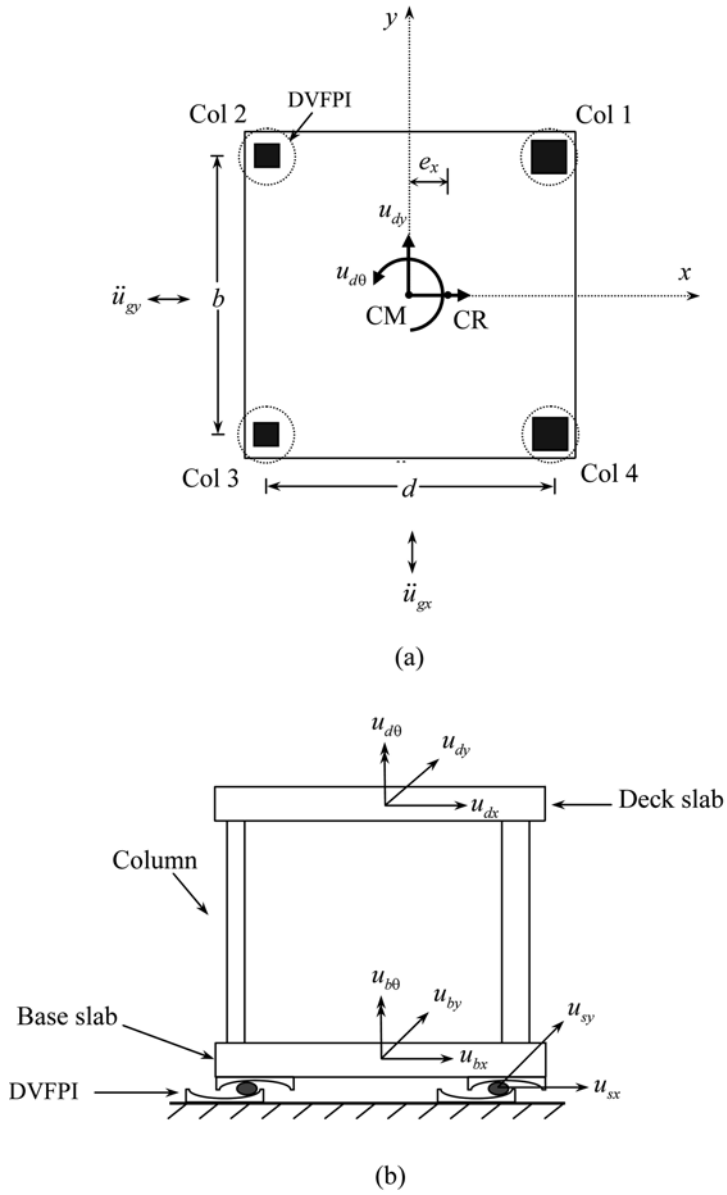

Fig. 2 Structural model: (a) plan, (b) elevation

massless, axially inextensible columns and the columns are connected to a rigid base slab. The CM is located at the geometrical centre of the deck slab, as the columns are modelled as massless and column masses are included in the slab mass. Each column has the same stiffness in the two principal directions. The stiffness distribution of the columns is symmetric about the *x*-axis but not about the *y*-axis, as a result, the structure exhibits a torsional effect when excited in the lateral *y*-direction. The system of isolators consists of an array of the DVFPI arranged between the foundation and the rigid base slab.

The dynamic behaviour of the system under consideration to earthquake excitation can be described by the following eight degrees of freedom: the two translational displacements, u_{dx} and u_{dy}, in orthogonal directions and rotation, $u_{d\theta}$, about vertical axes of the centre of deck mass relative to the base mass; the two translational displacements, u_{bx} and u_{by}, in orthogonal directions and rotation, $u_{b\theta}$, about vertical axes of the centre of base mass relative to the ground; and the u_{sx} and u_{sy}, the displacements of slider relative to ground in x- and y-directions, respectively as shown in Fig. 2(b).

Let k_{xi} and k_{yi}, $i = 1, 2 \ldots N$ denote the lateral stiffnesses of the ith column in x- and y-directions, respectively, where N denote the number of columns in each direction. The total lateral stiffness of the system in each direction, K_x, K_y is given by

$$K_x = \sum_{i=1}^{N} k_{xi}; \quad K_y = \sum_{i=1}^{N} k_{yi} \tag{12}$$

and the total torsional stiffness defined about the centre of mass (CM) of the deck is

$$K_\theta = \sum_{i=1}^{N} (k_{xi} Y_i^2 + k_{yi} X_i^2) \tag{13}$$

where X_i and Y_i denote the x- and y-co-ordinates of the ith column with respect to the centre of mass of the deck slab, respectively. In Eq. (13) the torsional stiffness of each individual column element with respect to its longitudinal axis has been neglected. The eccentricity between the CM of the deck slab and the static centre of resistance (CR) of the columns is given by

$$e_x = \frac{1}{K_y} \sum_{i=1}^{N} (k_{yi} X_i) \tag{14}$$

Corresponding to the translational and rotational modes, the three uncoupled modal frequencies of the superstructure will be equal to

$$\omega_x = \sqrt{\frac{K_x}{m_d}}; \quad \omega_y = \sqrt{\frac{K_y}{m_d}}; \quad \omega_\theta = \sqrt{\frac{K_\theta}{m_d r_d^2}} \tag{15}$$

in which, r_d is the radius of gyration of the deck slab about the vertical axis through the CM. The frequencies ω_x, ω_y and ω_θ may be interpreted as the natural frequencies of the fixed-base system if it were torsionally uncoupled but, m_d, K_x, K_y and K_θ are the same as in the coupled system. The torsional mass of the deck and the base mass are varied to provide various uncoupled torsional to lateral frequency ratios. This can be achieved by varying the position of the lumped mass with respect to the CM.

Let k_{bi}, $i = 1, 2 \ldots NB$ denote the lateral stiffnesses of the ith DVFPI isolator in lateral directions, where NB denote the number of isolators in each direction. The total lateral stiffness of the jth sliding surfaces of the isolation system, K_{bj}, is given by

$$K_{bj} = \sum_{i=1}^{N} k_{bji} \tag{16}$$

where k_{bji} represent the lateral stiffness of jth sliding surface of the ith isolator which is same in both x- and y-directions due to isotropic nature of the isolator. The torsional stiffness of the isolation

system defined about the CM of the base slab is given by

$$K_{b\theta} = \sum_{i=1}^{NB} (k_{b1i} Y_{bi}^2 + k_{b1i} X_{bi}^2) \tag{17}$$

where, X_{bi} and Y_{bi} denote the x- and y-co-ordinates of the ith DVFPI with respect to the centre of mass of the base slab, respectively. The displacement of top sliding surface of ith DVFPI can be expressed in terms of displacement of CM of the base mass

$$u_{bxi} = u_{bx} - Y_{bi} u_{b\theta} \quad \text{and} \quad u_{byi} = u_{by} + X_{bi} u_{b\theta} \tag{18a, 18b}$$

The horizontal displacements of the slider, x_{ji} and y_{ji} of the ith DVFPI relative to the centre of the top and bottom sliding surfaces can be expressed from Eq. (7) as

$$x_{1i} = u_{bxi} - u_{sx} \quad \text{and} \quad y_{1i} = u_{byi} - u_{sy} \tag{19a, 19b}$$

$$x_{2i} = u_{sx} \quad \text{and} \quad y_{2i} = u_{sy} \tag{19c, 19d}$$

Here, the torsional stiffness of each individual bearing is assumed to be small and is neglected. Moreover, for the purpose of simplification it is assumed that the bearings are symmetrically placed such that there is no eccentricity between the centre of mass and the centre of resistance.

The isolator stiffness eccentricity, e_{bx} between the CR and CM of the base slab is given by

$$e_{bx} = \frac{1}{K_b} \sum_{i=1}^{NB} (k_{b1i} X_{bi}) \tag{20}$$

The two uncoupled base isolation frequencies are defined as

$$\omega_b = \sqrt{\frac{K_{b1}}{m_d + m_b}} \quad \text{and} \quad \omega_{b\theta} = \sqrt{\frac{K_{b\theta}}{m_d r_d^2 + m_b r_b^2}} \tag{21}$$

Here, r_b is the radius of gyration of the base about the vertical axis through the CM. The values of ω_b and $\omega_{b\theta}$ are used to characterize the stiffness characteristics of the isolation device.

It is worth noting that the eccentricity of the DVFPI isolation system does remain constant during earthquake ground motion. It changes with isolator displacement as the stiffness of the isolation system is a function of isolator displacement. Depending upon the displacement of the isolators, the variations in isolation eccentricity can be significant (Eq. (20)).

4. Governing equations of motion

The governing equations of motion for the three-dimensional superstructure, base mass and slider are expressed in matrix form as

$$[M]\{\ddot{u}_d\} + [C]\{\dot{u}_d\} + [K]\{u_d\} = -[M][r]\{\ddot{u}_b + \ddot{u}_g\} \tag{22}$$

$$[M_b]\{\ddot{u}_b\} + [K_{b1}]\{u_1\} + \{F_1\} - [C]\{\dot{u}_d\} - [K]\{u_d\} = -[M_b][r]\{\ddot{u}_g\} \tag{23}$$

$$[M_s]\{\ddot{u}_s\} - [K_{b1}]\{u_1\} - \{F_1\} + [K_{b2}]\{u_2\} + \{F_2\} = -[M_s][r]\{\ddot{u}_g\} \tag{24}$$

wherein $[M],[K]$ and $[C]$ are the lumped mass, stiffness and damping matrices, respectively, corresponding to the DOF at the deck; $\{u_d\} = \{u_{dx}, u_{dy}, u_{d\theta}\}^T$ is the vector of displacements at the deck relative to the base mass; $\{u_b\} = \{u_{bx}, u_{yb}, u_{b\theta}\}^T$ is the vector of displacements at the base mass; $\{\ddot{u}_g\} = \{\ddot{u}_{gx}, \ddot{u}_{gy}\}^T$ is the vector of ground accelerations, $\ddot{u}_{gx}$ and $\ddot{u}_{gy}$ are the ground accelerations in the x- and y-directions, respectively; and $[r]$ is the earthquake influence coefficient matrix; $[M_b]$ is the lumped mass matrix corresponding to the DOF at the base mass; $[M_s]$ is the lumped mass matrix corresponding to the DOF at the slider; $[M_{bj}]$ is the stiffness matrices of jth sliding surfaces of the isolation system, respectively; $\{F_1\} = \{F_{x2}, F_{y2}, F_\theta\}^T$ and $\{F_2\} = \{F_{x2}, F_{y2}\}^T$ are the vector of frictional forces at top and bottom sliding surfaces of the isolation system, respectively, F_{xj} and F_{yj} are the frictional forces in the x- and y-directions, respectively on the corresponding sliding surface, F_θ is the frictional force about the vertical axis; The damping matrix $[C]$ is not explicitly known. It is constructed from the assumed modal damping for the fixed-base structure using its mode shapes and frequencies. If α is the angle of incidence of ground acceleration wave with respect to the x-axis, then the matrix $[r]$ is given by

$$[r] = \begin{bmatrix} \cos\alpha & -\sin\alpha \\ \sin\alpha & \cos\alpha \\ 0 & 0 \end{bmatrix} \tag{25}$$

The stiffness matrices $[K]$ and $[K_{bj}]$ are written as

$$[K] = \sum_{i=1}^{N} [a_i^T][k_i][a_i] \tag{26}$$

where,

$$[k_i] = \begin{bmatrix} k_{xi} & 0 & 0 \\ 0 & k_{yi} & 0 \\ 0 & 0 & 0 \end{bmatrix} \quad \text{and} \quad [a_i] = \begin{bmatrix} 1 & 0 & -y_i \\ 0 & 1 & x_i \\ -y_i & x_i & 1 \end{bmatrix} \tag{27, 28}$$

$$[K_{bj}] = \sum_{i=1}^{NB} [a_{bi}^T][k_{ji}][a_{bi}] \tag{29}$$

where,

$$[k_{ji}] = \begin{bmatrix} k_{bji} & 0 & 0 \\ 0 & k_{bji} & 0 \\ 0 & 0 & 0 \end{bmatrix} \quad \text{and} \quad [a_{bi}] = \begin{bmatrix} 1 & 0 & -y_{bi} \\ 0 & 1 & x_{bi} \\ -y_{bi} & x_{bi} & 1 \end{bmatrix} \tag{30, 31}$$

in which $[a_i]$ and $[a_{bi}]$ are the transformation matrices of the ith column and the isolator, respectively.

5. Solution of equations of motion

Due to non-linear force-deformation behaviour of the DVFPI and significant difference in damping of superstructure and the isolation system the governing equations of motion of the base isolated structure cannot be solved using the classical modal superposition technique. Therefore, they are solved in the incremental form using Newmark's step-by-step method assuming linear variation of acceleration over small time interval in this study. The frictional forces are obtained by hysteretic model, which is a continuous model of the frictional force proposed by Constantinou *et al.* (1990), using Wen (1976) equation. In the hysteretic model, the interaction between the frictional forces has been expressed by coupling of the hysteretic displacements components in two directions (Park *et al.* 1986). Due to highly non-linear behaviour of the system, and the strong influence of initial conditions at each time-step on the numerical solution, a very small time step of the order of 1×10^{-5} has been found suitable for step-by-step solution. The complete procedure of the solution of equations of motion can be found in Panchal *et al.* (2009).

6. Parametric study

The response of asymmetric building isolated with the DVFPI to the selected ground motions is investigated with respect to the following parameters: eccentricity ratio of the superstructure, e_x/d, ratio of uncoupled torsional to lateral frequencies of the superstructure, ω_θ/ω_x, uncoupled time period of the superstructure, T_x, and mass ratio, m_b/m_d. Since these parameters predominantly influence the torsional coupling and base isolation characteristics, the range of these parameters was carefully selected in order to obtain a better understanding of the influence of the system parameters on torsional coupling. The specifications for the values of the other parameters are: lateral dimension, $b = d = 10.0$ m; number of the DVFPI isolators is 4; modal damping for the superstructure is taken as 2 per cent of the critical damping for all modes; and the ratio of mass of slider to mass of base slab, m_s/m_b is taken as 0.001.

Six response quantities, viz. peak rotation of deck slab, u_θ, peak rotation of base slab, $u_{b\theta}$, peak base torque, peak resultant isolator displacement, u_{br}, peak base shear in y-direction and deck corner displacement magnification (Nagarajalah *et al.* 1993a) are considered for the present study. The deck corner displacement provides the magnitude of deformation due to the combined effect of translation and torsion. By investigating the extent of magnification of deck corner displacement in comparison with the displacement at the centre of mass of the deck, the effect of torsional coupling can be qualitatively evaluated. For this purpose, the corner displacement magnification is utilized. It is defined as the ratio of peak deck corner displacement (relative to base) to peak displacement at the CM (relative to base).

The parametric variations in isolation eccentricity, e_{bx}/d, and the ratio of uncoupled torsional to lateral frequencies of the isolator, $\omega_{b\theta}/\omega_b$ are not presented explicitly due to continuous variation in restoring force of the DVFPI and hence in e_{bx}/d and $\omega_{b\theta}/\omega_b$ during earthquake ground motion. However, the present formulation includes these variations in its mathematical model consequently these effects are automatically reflected in the analysis results.

The structural response is obtained under a set of six far-fault ground motions having magnitude ranging from 6.6 to 7.0 recorded at a distance of 8 to 16 km on firm soil or rock site. The ground motions selected are representative of typical Large-Magnitude-Small-distance ground

Table 1 Details of earthquake ground motions used in the study

Earthquake	Magnitude	Applied in x-direction		Applied in y-direction		Distance from surface projection of the fault (km)
		Component	PGA (g)	Component	PGA (g)	
Imperial Valley, 1940 (El Centro)	6.9	180	0.313	270	0.215	8.0
Loma Prieta, 1989 (Saratoga Aloha Ave.)	6.9	000	0.512	090	0.324	9.0
Superstition Hills, 1987 (El Centro Imp. Co. Center)	6.5	000	0.358	090	0.258	13.9
Loma Prieta, 1989 (Capitola)	6.9	000	0.529	090	0.443	14.5
Northridge, 1994 (Canoga Park - Topanga Canyon)	6.7	196	0.420	106	0.356	15.8
Northridge, 1994 (Northridge-Saticoy St.)	6.7	180	0.477	090	0.368	13.3

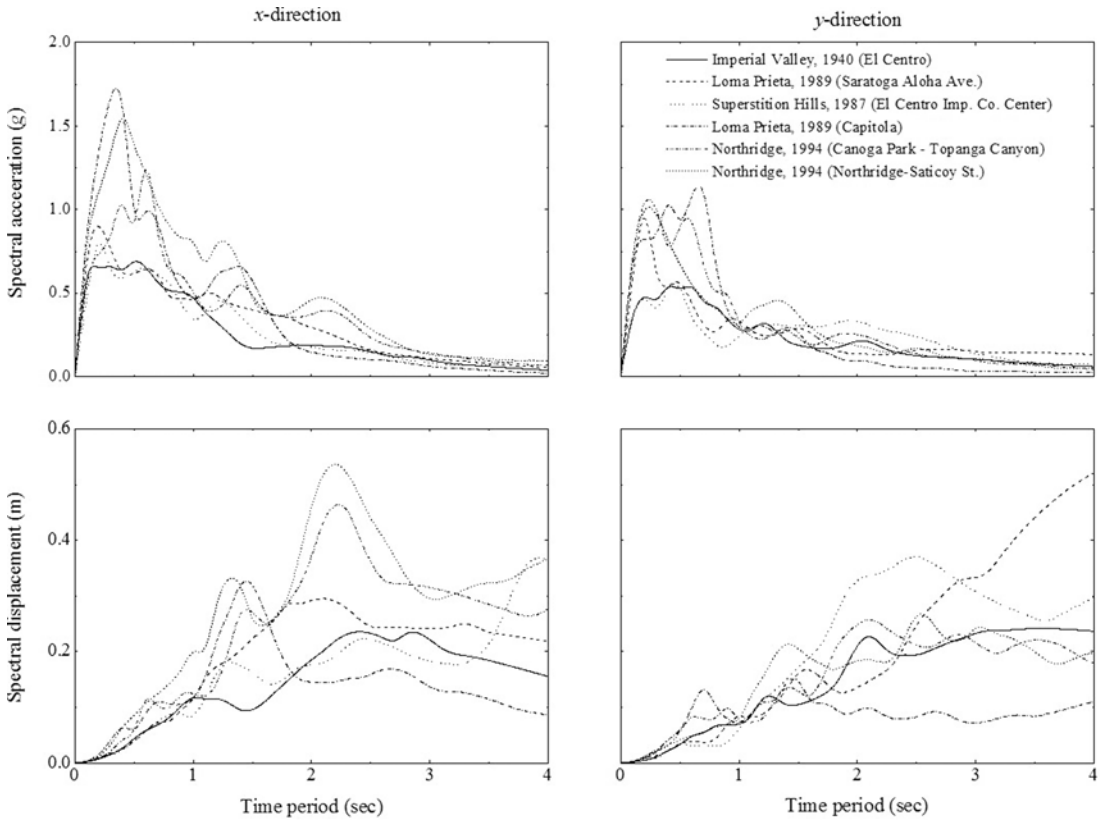

Fig. 3 Acceleration and displacement spectra of the six far-fault ground motions for 5 per cent damping

Table 2 Properties of the different DVFPI design cases

Group	Case	T_1 (sec)	T_2 (sec)	T_c (sec)	μ_1	μ_2	μ_c	Remark
A ($T_1 \neq T_2$, $\mu_1 \neq \mu_2$)	A_1	1.5	2	2.5	0.04	0.07	0.06	$T_1<T_2$; $\mu_1<\mu_2$
	A_2	1.5	2	2.5	0.07	0.053	0.06	$T_1<T_2$; $\mu_1>\mu_2$
	A_3	2	1.5	2.5	0.07	0.04	0.06	$T_1>T_2$; $\mu_1>\mu_2$
	A_4	2	1.5	2.5	0.053	0.07	0.06	$T_1>T_2$; $\mu_1<\mu_2$
B ($T_1 = T_2$, $\mu_1 = \mu_2$)	B	1.77	1.77	2.5	0.06	0.06	0.06	$T_1=T_2$; $\mu_1=\mu_2$
C ($T_1 = T_2$, $\mu_1 \neq \mu_2$)	C_1	1.77	1.77	2.5	0.05	0.07	0.06	$T_1=T_2$; $\mu_1<\mu_2$
	C_2	1.77	1.77	2.5	0.07	0.05	0.06	$T_1=T_2$; $\mu_1>\mu_2$
D ($T_1 \neq T_2$, $\mu_1 = \mu_2$)	D_1	1.5	2	2.5	0.06	0.06	0.06	$T_1<T_2$; $\mu_1=\mu_2$
	D_2	2	1.5	2.5	0.06	0.06	0.06	$T_1>T_2$; $\mu_1=\mu_2$

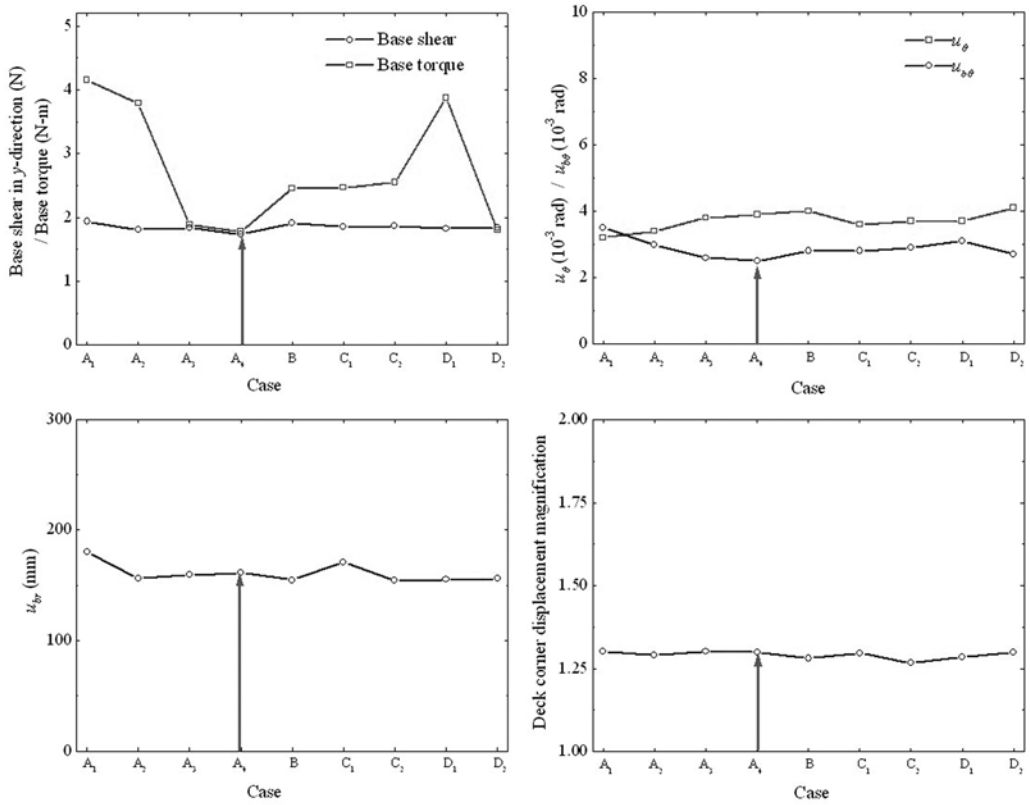

Fig. 4 Comparison of median response quantities for various cases of the DVFPI design

motion records. The characteristics of these earthquakes are listed in Table 1 and their displacement and acceleration spectra for 5 per cent damping are shown in Fig. 3. The stronger component among the two lateral components is applied in a direction perpendicular to the direction of eccentricity.

In order to study the optimum performance of the DVFPI supporting asymmetric building, nine different isolator design cases have been considered as listed in Table 2. These are categorised into four groups depending on the isolator geometry and coefficient of friction of top and bottom sliding surface as (a) unequal isolator geometry and unequal coefficient of friction, (b) equal isolator geometry and equal coefficient of friction, (c) unequal isolator geometry and equal coefficient of friction, and (d) equal isolator geometry and unequal coefficient of friction of the two sliding surfaces. The isolators have been design to give same combined initial time period, T_c, and coefficient of friction, μ_c, for all design cases to make meaningful comparison among them. The median response of the example system for all design cases are plotted in Fig. 4. As observed from the figure that most of the response quantities minimize for A_4 Case, i.e., the DVFPI with higher initial time period and lesser coefficient friction of the top sliding surface relative to the bottom one.

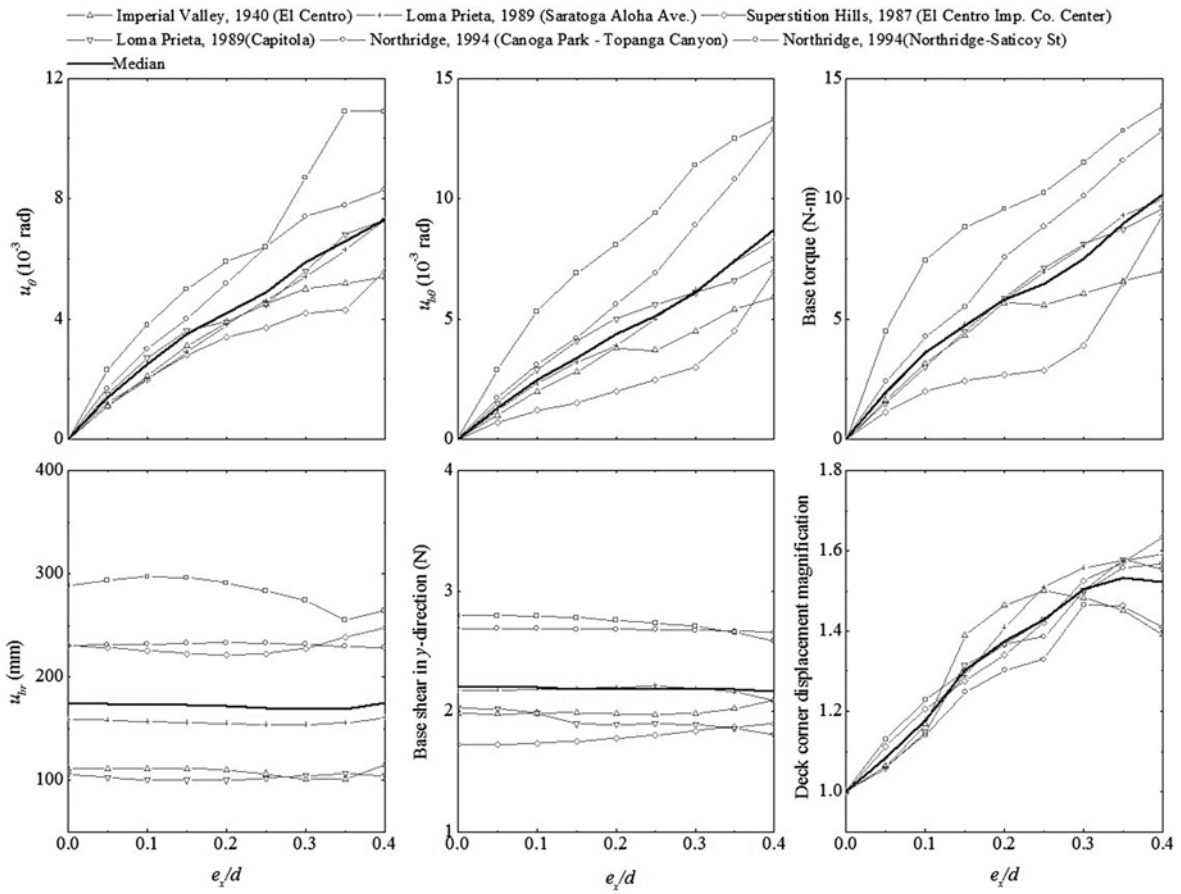

Fig. 5 Effect of e_x/d on the response of the asymmetric building isolated with the DVFPI; T_x = 1 sec, ω_θ/ω_x = 1.0, m_b/m_d = 1.0, T_1 = 1.5 sec, T_2 = 2.0 sec, μ_1 = 0.04, μ_2 = 0.07, d_1 = 0.3 and d_2 = 0.3

This observation suggests that in order to optimize the performance of the DVFPI for torsion the top sliding surface should be made initially softer and smoother than the bottom surface. Moreover, it should be noted that initially stiffer and smoother top sliding surface (Case A_1) amplifies the responses.

6.1 Effect of superstructure eccentricity

The superstructure stiffness eccentricity, e_x/d is the most important parameter causing torsional coupling and torsional motions. Fig. 5 is plotted to show the effects of superstructure eccentricity in torsionally coupled structure isolated with the DVFPI (T_1 = 1.5 sec, T_2 = 2.0 sec, μ_1 = 0.04, μ_2 = 0.04, d_1 = 0.3 m and d_2 = 0.3 m), under the six selected ground motions. The median response of the six earthquakes is also plotted in the figure. The superstructure eccentricity is varied from a symmetric case, e_x/d = 0 to asymmetric case, e_x/d = 0.4. As shown in figure that the eccentricity increases torsional responses, i.e., the deck slab rotation, base slab rotation and base torque.

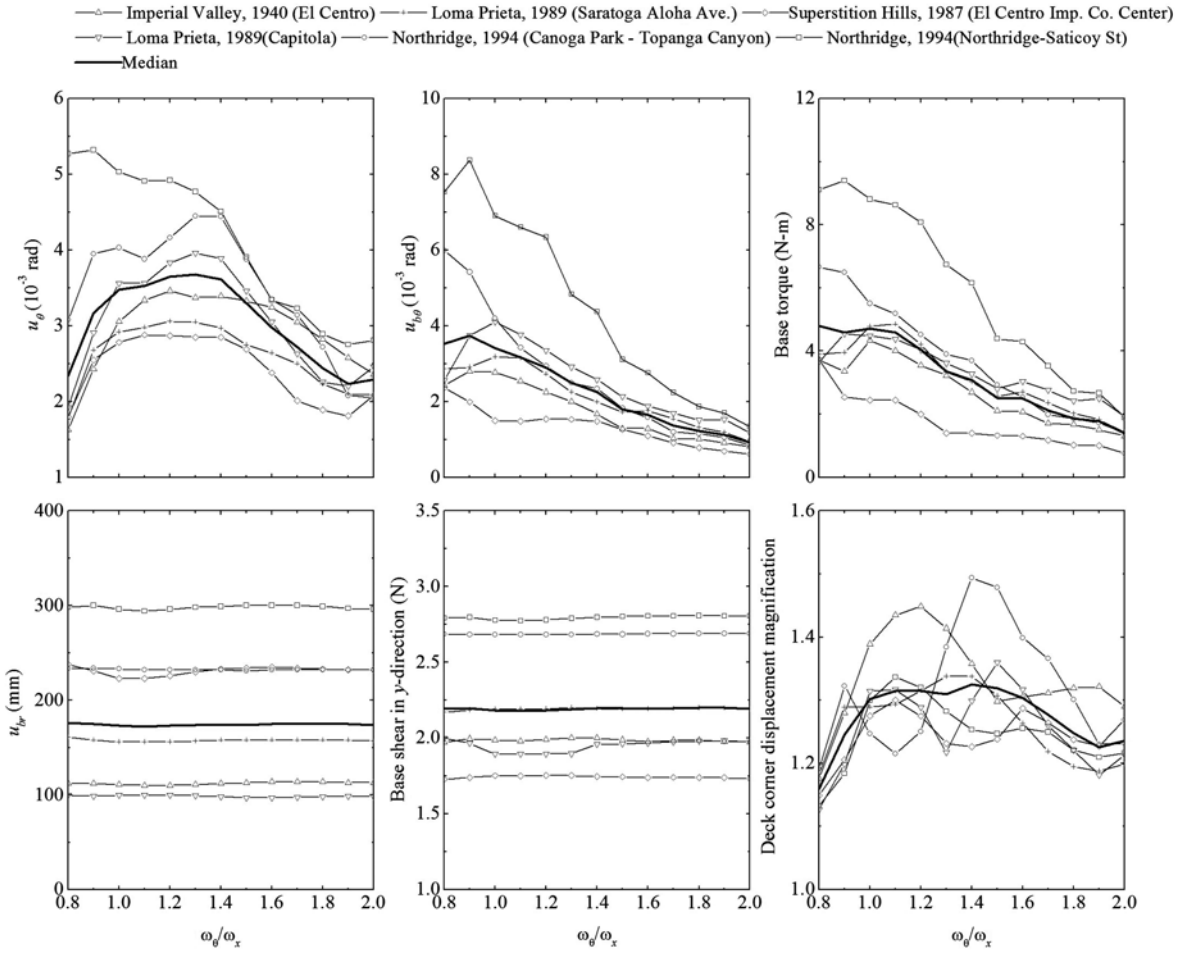

Fig. 6 Effect of ω_θ/ω_x on the response of the asymmetric building isolated with the DVFPI; T_x = 1 sec, e_x/d = 0.15, m_b/m_d = 1.0, T_1 = 1.5 sec, T_2 = 2.0 sec, μ_1 = 0.04, μ_2 = 0.07, d_1 = 0.3 and d_2 = 0.3

However, the lateral responses, i.e., resultant isolator displacement and peak base shear are not much influenced by superstructure eccentricity. Further, the deck corner displacement magnification also increases with eccentricity as expected.

6.2 Effect of torsional to lateral frequency ratio of the superstructure

The ratio of uncoupled torsional to lateral frequency is an important parameter in the behaviour of the asymmetric buildings; that is, highly influences the response of such systems. As shown in Fig. 6 with the increase of ω_θ/ω_x in the range of $0.8 \le \omega_\theta/\omega_x \le 1$, the deck corner magnification and deck slab rotation increases, remains nearly constant in the range of $1 \le \omega_\theta/\omega_x \le 1.5$ and decreases as the system become stiffer. Base torque and base rotation on the other hand decreases continuously with the increase of ω_θ/ω_x. Further, the lateral responses remain essentially insensitive to the variation of ω_θ/ω_x.

Thus, the e_x/d and ω_θ/ω_x have opposing effects on the coupled lateral-torsional response. It will

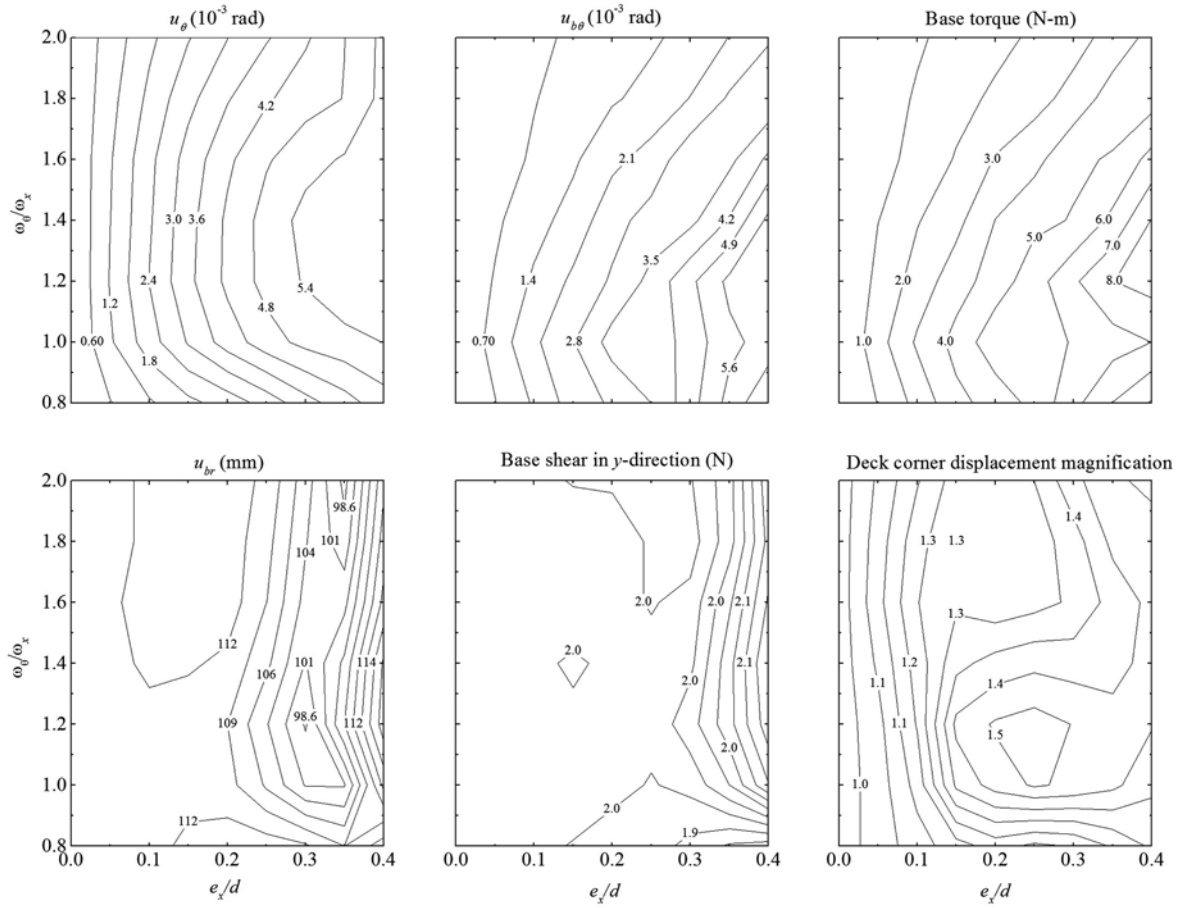

Fig. 7 Combined effect of e_x/d and ω_θ/ω_x on the response of the asymmetric building isolated with the DVFPI; T_x = 1 sec, m_b/m_d = 1.0, T_1 = 1.5 sec, T_2 = 2.0 sec, μ_1 = 0.04, μ_2 = 0.07, d_1 = 0.3 and d_2 = 0.3

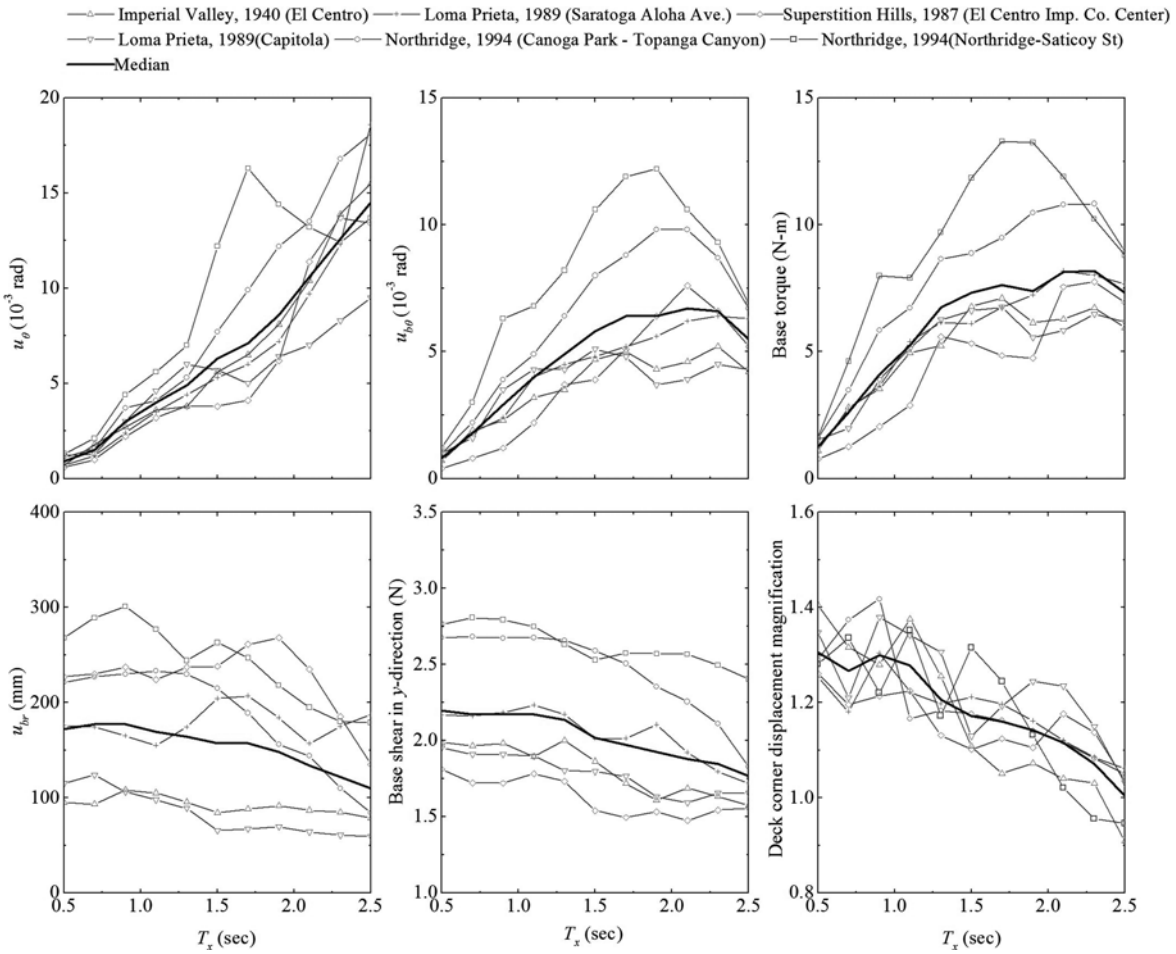

Fig. 8 Effect of T_x on the response of asymmetric building isolated with the DVFPI; e_x/d = 0.15, ω_θ/ω_x = 1, m_b/m_d = 1.0, T_1 = 1.5 sec, T_2 = 2.0 sec, μ_1 = 0.04, μ_2 = 0.07, d_1 = 0.3 and d_2 = 0.3

be interesting to examining the combined effect of these two parameters. This is explained by three dimensional plots of response for Imperial Valley, 1940 (El Centro) earthquake ground motion for the aforesaid combination in Fig. 7. The figure indicates that the superstructure eccentricity increases the torsional response quite rapidly than the uncoupled torsional to lateral frequency ratio suppresses them. This observation suggests that it is advisable to control the eccentricity rather than increasing the torsional stiffness to reduce torsional responses.

6.3 Effect of uncoupled time period of superstructure

In Fig. 8, response of the DVFPI isolated asymmetric building is plotted for different values of superstructure time period, T_x. Increasing the T_x thereby making superstructure flexible in horizontal direction all the torsional responses increase and lateral responses decrease. The deck corner displacement magnification on the other hand decreases due to increase in deck lateral displacement with the increase in superstructure flexibility.

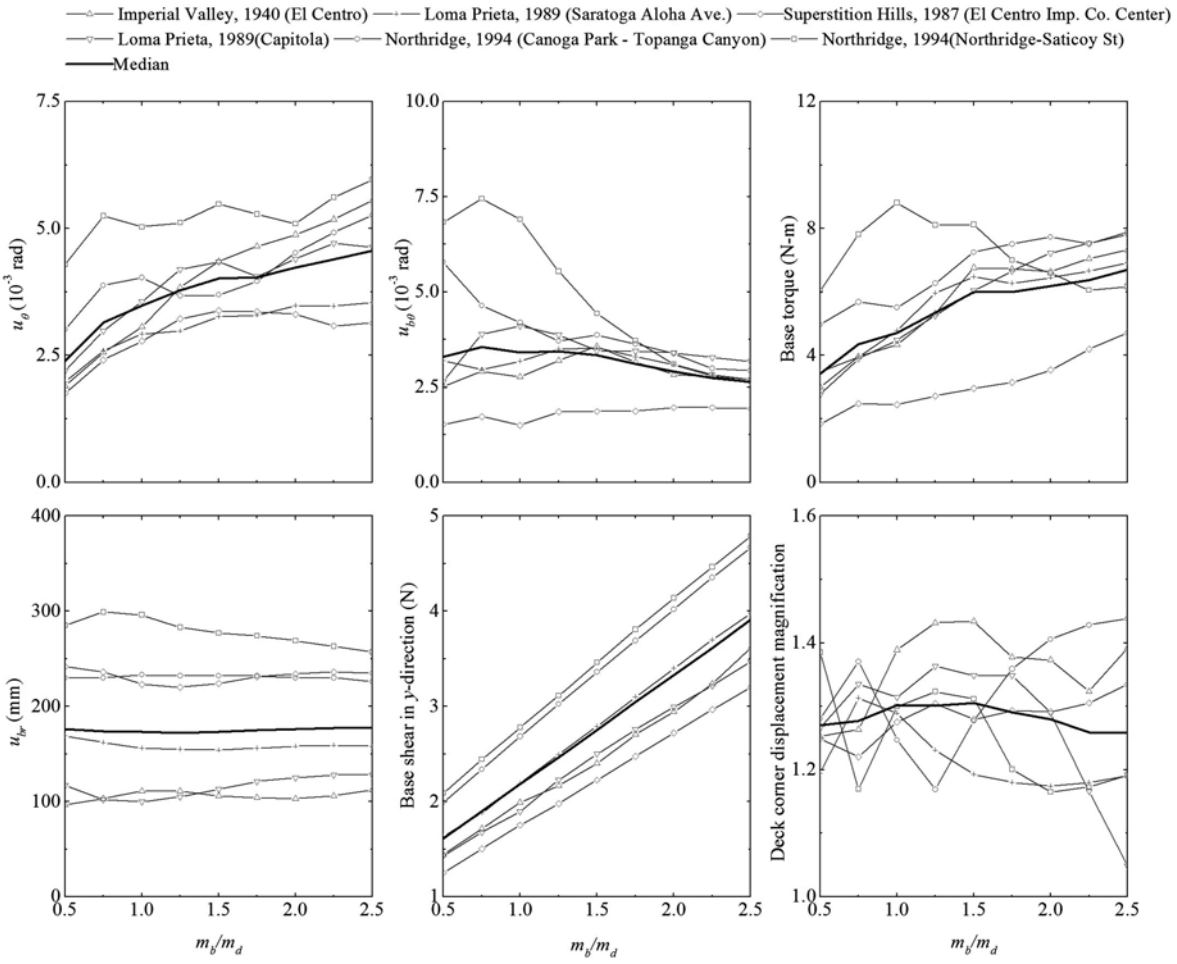

Fig. 9 Effect of m_b/m_d on the response of the asymmetric building isolated with the DVFPI; T_x = 1, e_x/d = 0.15, ω_θ/ω_x = 1, T_1 = 1.5 sec, T_2 = 2.0 sec, μ_1 = 0.04, μ_2 = 0.07, d_1 = 0.3 and d_2 = 0.3

6.4 Effect of mass ratio

Fig. 9 depicts the influence of variation in mass ratio, m_b/m_d, on the structural response. The base shear is highly influenced by variation of m_b/m_d. This is expected as the base shear is directly proportional to the weight of the building. The base torque and deck slab rotation increases slowly with the increases of mass ratio. However, the base rotation, deck corner displacement magnification and the resultant isolator displacement remains almost same for all values of mass ratio.

6.5 Effect of angle of incidence

In Fig. 10, the variation of the structural response is plotted against the angle of incidence, α for the six ground motions. The figure indicates that the responses are moderately influenced by

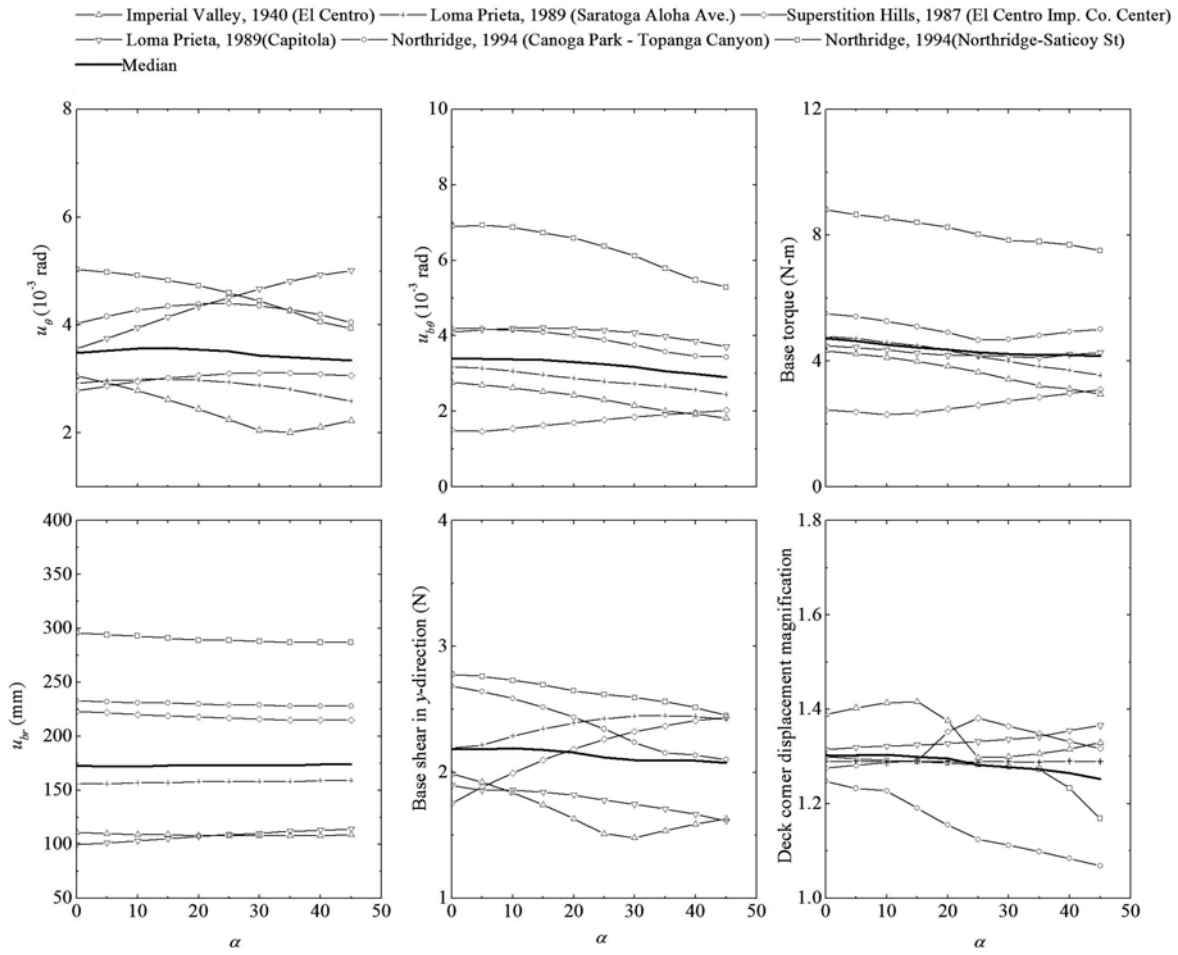

Fig. 10 Effect of α on the response of the asymmetric building isolated with the DVFPI; $T_x = 1$, $e_x/d = 0.15$, $\omega_\theta/\omega_x = 1$, $m_b/m_d = 1.0$, $T_1 = 1.5$ sec, $T_2 = 2.0$ sec, $\mu_1 = 0.04$, $\mu_2 = 0.07$, $d_1 = 0.3$ and $d_2 = 0.3$

the angle of incidence of ground acceleration with respect to the principal direction of the structure.

6.6 Influence of isolator geometry

The isolator geometry of the DVFPI can be completely defined by parameter b_i and d_i. As the initial time period, T_i is directly proportional to b_i, the influence of isolator geometry is studied by varying d_1, d_2 and T_1, T_2. The value of d_i and T_i are varied within range of 0.1-0.5 m and 1.0-2.0 sec, respectively. It should be noted that the reciprocal of d_i is the FVF_i of corresponding sliding surface. To study the effect of d_1 and d_2, other parameters are kept equal, i.e., $\mu_1 = \mu_2 = \mu_c$ and $T_1 = T_2 = T_c$. Fig. 11 shows three dimensional plots of response quantities considered for Imperial Valley, 1940 (El Centro) ground motion. It is seen that for the given value of d_1 the torsional response is independent of d_2. Figure also suggests that for lower value of d_1 (i.e., higher value of the FVF_1) the

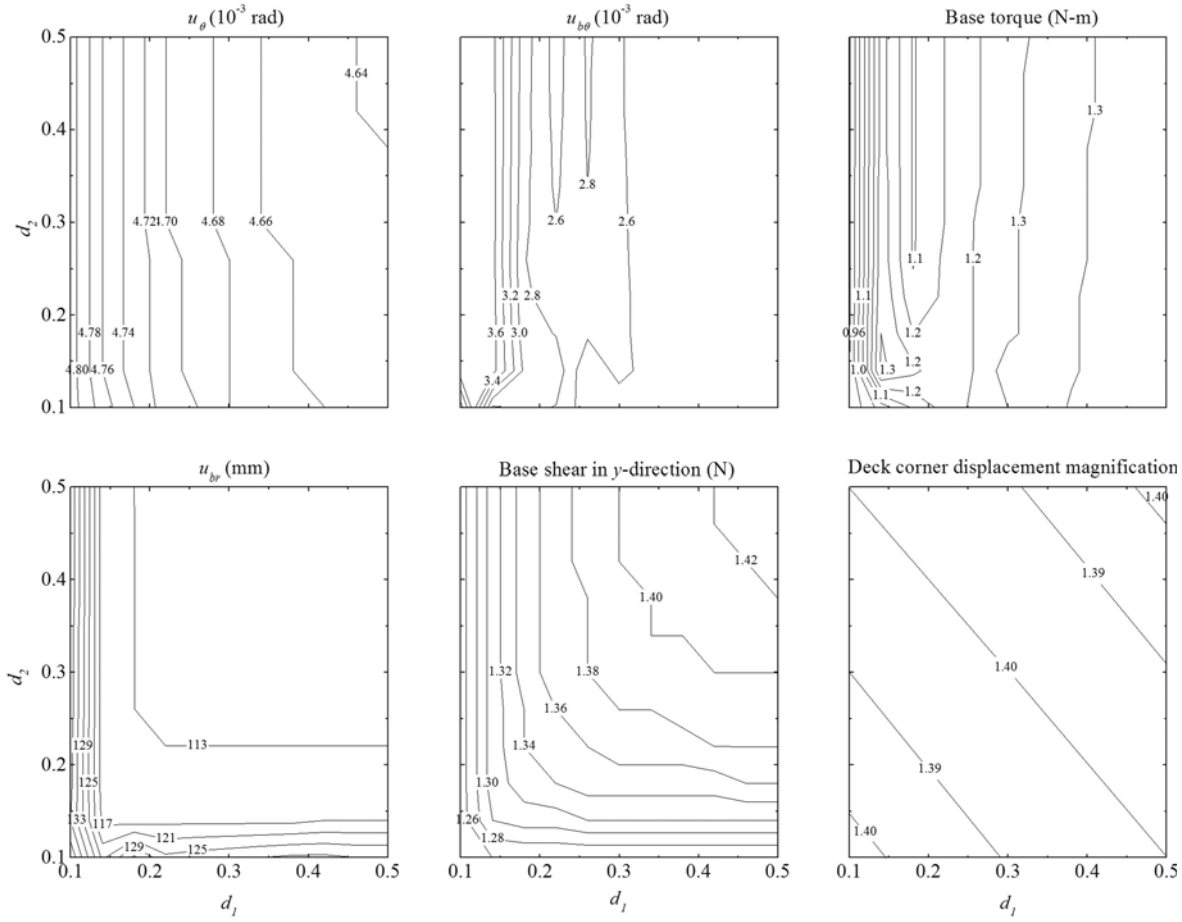

Fig. 11 Variations in peak response quantities of the DVFPI isolated torsionally coupled building for different values of T_1 and T_2; T_x = 1, e_x/d = 0.15, ω_θ/ω_x = 1, m_b/m_d = 1.0, μ_1 = 0.04, μ_2 = 0.07, d_1 = 0.3 and d_2 = 0.3

lateral response is essentially independent of d_2 (i.e., the FVF_2). However, for higher value of d_1, the lateral responses are sensitive to d_2. Further, the deck corner displacement magnification is not influenced by variations in FVFs.

Fig. 12 portrays the influence of initial time period of top and bottom sliding surface on the seismic response of the DVFPI. As shown in figure, the response varies more rapidly within small range of T_1 and T_2 showing its sensitivity for lower value of initial time period of both sliding surfaces. For higher value of T_1, the torsional responses are essentially independent of T_2.

6.7 Influence of coefficient of friction

The influence of coefficient of friction is studied by varying μ_1 and μ_2 at the two sliding surfaces in the range of 0.01-0.07, keeping other parameters constant, i.e., $T_1 = T_2 = T_c$ and $d_1 = d_2 = 0.3$ m and is shown in Fig. 13. The response is found sensitive for all values of coefficient of friction. Increasing friction coefficient, the limiting value of sliding force increases. As a result, more force

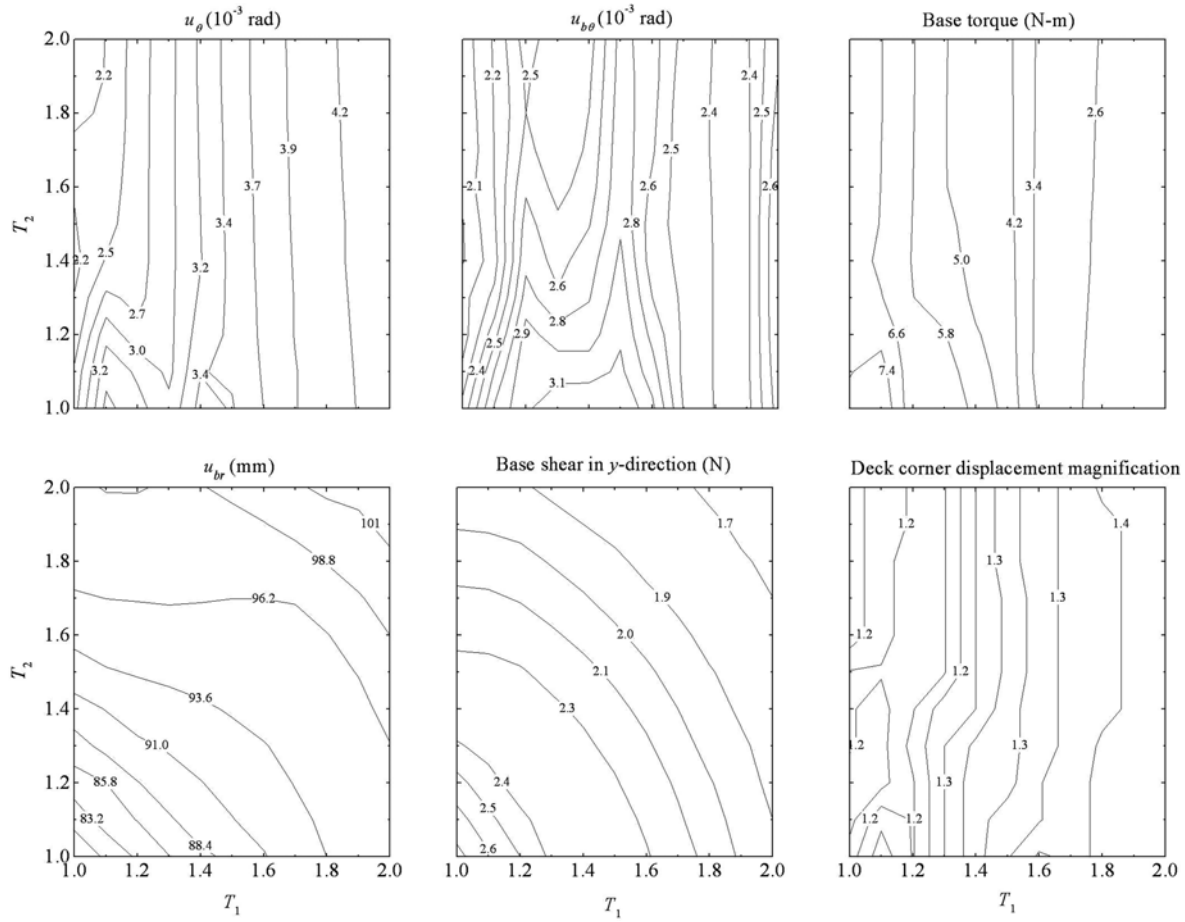

Fig. 12 Variations in peak response quantities of the DVFPI isolated torsionally coupled building for different values of d_1 and d_2; $T_x = 1$, $e_x/d = 0.15$, $\omega_\theta/\omega_x = 1$, $m_b/m_d = 1.0$, $T_1 = 1.5$ sec, $T_2 = 2.0$ sec, $\mu_1 = 0.04$, $\mu_2 = 0.07$

will be transmitted by the sliding surfaces into the superstructure which in turn magnifies all responses quantities except resultant isolator displacement.

7. Conclusions

The non-linear response of a torsionally coupled system isolated with double variable frequency pendulum system (DVFPI) to bilateral far-fault ground motions is obtained by considering the interaction of frictional forces in two orthogonal directions. The response behaviour of the torsionally coupled system is studied for a set of important parametric variations. The criterion to optimize the performance of the DVFPI for coupled lateral-torsional response is proposed. Further, the influences of the initial time period, the coefficient of friction and the frequency variation factors at the two sliding surface are investigated. The conclusions of this study are based on the

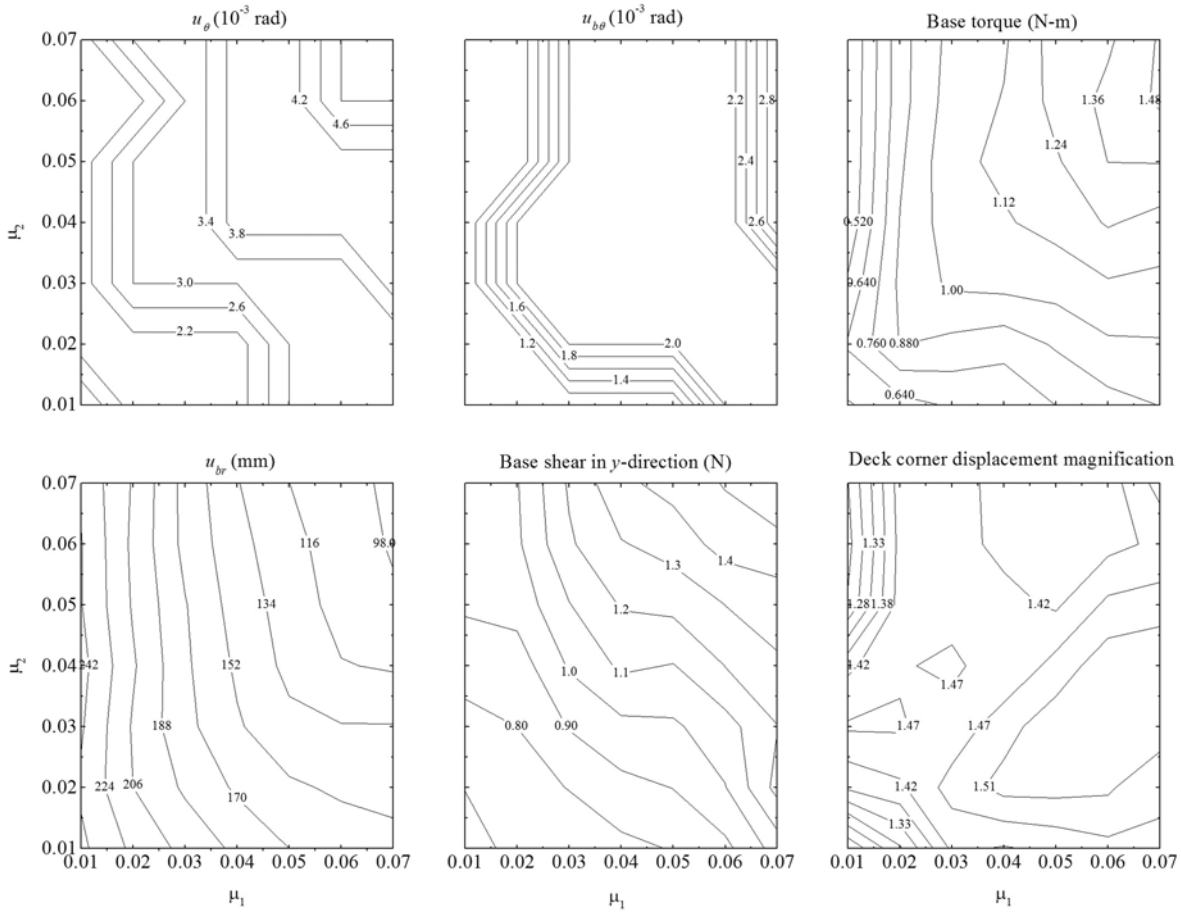

Fig. 13 Variations in peak response quantities of the DVFPI isolated torsionally coupled building for different values of μ_1 and μ_2; $T_x = 1$, $e_x/d = 0.15$, $\omega_\theta/\omega_x = 1$, $m_b/m_d = 1.0$, $T_1 = 1.5$ sec, $T_2 = 2.0$ sec, $d_1 = 0.3$ and $T_x = 0.3$

assumption of stable and predictable sliding friction at the sliding interfaces, which are configured as depicted in Fig. 1(a). As discussed earlier in this paper, this may not be possible due to high concentration of pressure at the sliding interface. The following conclusions may be drawn from the trend of numerical results of the present study:

1. For the optimum performance of the DVFPI supporting asymmetric building, the top sliding surface should be designed initially softer and smoother.
2. The superstructure eccentricity magnifies the torsional response and the uncoupled torsional to lateral frequency ratio reduces it. However, the superstructure eccentricity increases the torsional response quite rapidly than the uncoupled torsional to lateral frequency ratio suppresses them. Therefore, the superstructure eccentricity should be control rather than making superstructure torsionally stiff.
3. The superstructure flexibility magnifies torsional response and reduces lateral responses and deck corner displacement magnification of the DVFPI system.
4. The torsional responses are not much influenced by the ratio of base mass to deck mass.

However, base shear increases significantly with the mass ratio.

5. The angle of incidence of the ground motions with respect to the principal direction of structure moderately influences the performance of the DVFPI system.
6. For the given value of frequency variation factor of top sliding surface of the DVFPI, the torsional response is independent of frequency variation factor of bottom sliding surface.
7. When the top sliding surface of the DVFPI is design to have lower initial time period, the torsional response becomes sensitive to the initial time period of bottom sliding surface. On the other hand, for higher value of initial time period of top sliding surface, the response is independent of the initial time period of bottom sliding surface.
8. The torsional response is significantly influenced by coefficient of friction of both sliding surfaces. Increasing coefficient of friction either at top or bottom or both sliding surfaces of the DVFPI torsional response magnifies considerably.

References

Buckle, I.G. (1986), "Development and application of base isolation and passive energy dissipation: A world review", *ATC-17, Applied Technology Council*, Redwood City, California.

Buckle, I.G. and Mayes, R.L. (1990), "Seismic isolation: History, application and performance-a world overview", *Earthq. Spectra,* **6**(2), 161-201.

Constantinou, M.C., Mokha, A.S. and Reinhorn, A.M. (1990), "Teflon bearings in base isolation II: Modelling", *J. Struct. Eng.*, ASCE, **116**(2), 455-474.

Eisenberger, M. and Rutenberg, A. (1986), "Seismic base isolation of asymmetric shear buildings", *Eng. Struct.*, **8**(1), 2-8.

Fan, F.G., Ahmadi, G. and Tadjbakhsh, I.G. (1990), "Multi-story base-isolated buildings under a harmonic ground motion-Part II: Sensitivity analysis", *Nucl. Eng. Des.*, **123**(1), 17-26.

Fenz, D.M. and Constantinou, M.C. (2006), "Behaviour of the double concave friction pendulum bearing" *Earthq. Eng. Struct. Dyn.*, **35**(11), 1403-1424.

Fenz, D.M. and Constantinou, M.C. (2008a), "Spherical sliding isolation bearings with adaptive behavior: Theory", *Earthq. Eng. Struct. Dyn.*, **37**(2), 163-183.

Fenz, D.M. and Constantinou, M.C. (2008b), "Spherical sliding isolation bearings with adaptive behavior: Experimental verification", *Earthq. Eng. Struct. Dyn.*, **37**(2), 185-205.

Jangid, R.S. (1995), "Seismic response of an asymmetric base isolated structure", *Comput. Struct.*, **60**(2), 261-267.

Jangid, R.S. and Datta, T.K. (1994) "Non-linear response of torsionally coupled base isolated structure", *J. Struct. Eng.*, ASCE, **120**(1), 1-22.

Jangid, R.S. and Kelly, J.M. (2000), "Torsional displacement in base-isolated buildings", *Earthq. Spectra*, **16**(2), 443-454.

Kasalanati, A., Reinhorn, A.M., Constantinou, M.C. and Sanders, D. (1997), "Experimental study of ball-in-cone isolation system", *Proc. Structures Congress* XV, ASCE, Portland, Oregon.

Kelly, J.M. (1986), "Aseismic base isolation: Review and bibliography", *Soil Dyn. Earthq. Eng.*, **5**(4), 202-216.

Kim, Y.S. and Yun, C.B. (2005), "Analysis and design of double friction pendulum systems for seismic isolation", *The Second International Conference on Structural Health Monitoring of Intelligent Infrastructure*, Korea.

Lee, D.M. (1980), "Base isolation for torsion reduction in asymmetric structure under earthquake loading", *Earthq. Eng. Struct. Dyn.*, **8**(4), 349-359.

Naeim, F. and Kelly, J.M. (1999), *Design of Seismic Isolated Structures: From Theory to Practice*, Wiley, New York.

Nagarajalah, S., Reinhorn, A.M. and Constantinou, M.C. (1993a), "Torsional coupling in sliding base isolated structures", *J. Struct. Eng.*, ASCE, **119**(1), 130-149.

Nagarajalah, S., Reinhorn, A.M. and Constantinou, M.C. (1993b), "Torsion in base isolated structures with elastomeric isolation systems", *J. Struct. Eng.*, ASCE, **119**(10), 2932-2951.
Pan, T.C. and Kelly, J.M. (1983), "Seismic response of torsionally coupled base isolated structures", *Earthq. Eng. Struct. Dyn.*, **11**(6), 749-770.
Park, Y.J., Wen, Y.K. and Ang, A.H.S. (1986), "Random vibration of hysteretic systems under bidirectional motions", *Earthq. Eng. Struct. Dyn.*, **14**(4), 543-557.
Pranesh, M. and Sinha, R. (2000), "VFPI: An isolation device for aseismic design", *Earthq. Eng. Struct. Dyn.*, **29**(5), 603-627.
Pranesh, M. and Sinha, R. (2004), "Behavior of torsionally coupled structures with variable frequency pendulum isolator", *J. Struct. Eng.*, ASCE, **130**(7), 1041-54.
Panchal, V.R., Jangid, R.S., Soni, D.P. and Mistry, B.B. (2009), "Response of double variable frequency pendulum isolator under triaxial ground excitations", *J. Earthq. Eng.* (in press).
Soni, D.P., Mistry, B.B., Jangid, R.S. and Panchal, V.R. (2009), "Seismic response of the double variable frequency pendulum isolator", *Struct. Control Health Monit*. (in press).
Tena-Colunga, A. and Escamilla-Cruz, J.L. (2007), "Torsional amplifications in asymmetric base- isolated structures", *Eng. Struct.*, **29**(2), 237-247.
Tena-Colunga, A. and Gomez-Soberon, L. (2002), "Torsional response of base-isolated structures due to asymmetries in the superstructure", *Eng. Struct.*, **24**(12), 1587-1599.
Tsai, C.S., Chiang, T.C. and Chen, B.J. (2005), "Experimental evaluation of piecewise exact solution for predicting seismic responses of spherical sliding type isolated structures", *Earthq. Eng. Struct. Dyn.*, **34**(9), 1027-1046.
Wen, Y.K. (1976), "Method for random vibration of hysteretic systems", *J. Eng. Mech. Div.*, ASCE, **102**(2), 249-263.
Zayas, V., Low, S. and Mahin, S. (1987), "The FPS system: Experimental report", *Report No. UCB/EERC-87-01*, *Earthquake Engineering Research Centre*, Berkeley, California.